# Structure-Based Design of Potent Aromatase Inhibitors by High-Throughput Docking

Fabiana Caporuscio,[†] Giulio Rastelli,[†] Carol Imbriano,[‡] and Alberto Del Rio*,[†]

[†]Dipartimento di Scienze Farmaceutiche, Università di Modena e Reggio Emilia, Via Campi 183, 41100 Modena, Italy
[‡]Dipartimento di Biologia, Università di Modena e Reggio Emilia, Via Campi 213/D, 41100 Modena, Italy

S *Supporting Information*

ABSTRACT: Cytochrome P450 aromatase catalyzes the conversion of androgen substrates into estrogens. Aromatase inhibitors (AIs) have been used as first-line drugs in the treatment of estrogen-dependent breast cancer in postmenopausal women. However, the search for new, more potent, and selective AIs still remains necessary to avoid the risk of possible resistances and reduce toxicity and side effects of current available drugs. The publication of a high resolution X-ray structure of human aromatase has opened the way to structure-based virtual screening to identify new small-molecule inhibitors with structural motifs different from all known AIs. In this context, a high-throughput docking protocol was set up and led to the identification of nanomolar AIs with new core structures.
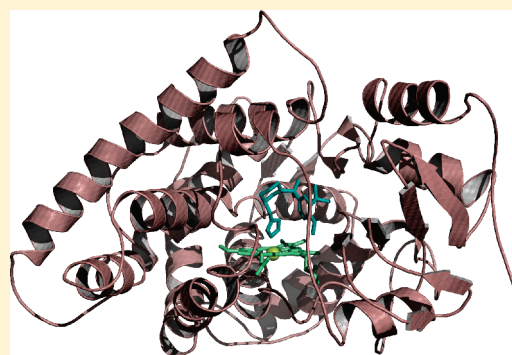
INTRODUCTION

Cytochrome P450 aromatase (CYP19) catalyzes the rate-limiting step in the biosynthesis of estrogens by the aromatization of the A ring of androgen precursors such as androstenedione (Chart 1) and testosterone. Despite the crucial role played by sex hormones in living organisms, estrogens are also involved in breast cancer occurrence and progression. In fact, estrogens bind to specific estrogen receptors (ERs) in the tumor and initiate a mitogenic signal. In premenopausal women, circulating estrogens are mainly synthesized in ovaries. However, in postmenopausal women, which are the majority of breast cancer patients, estrogens are produced in nonovarian tissue such as breast tissue or are synthesized peripherally by aromatase.[1]

Endocrine therapy controlling estrogen production in estrogen receptor positive (ER+) tumors has been the standard therapy in breast cancer. Selective estrogen receptor modulators (SERMs) block the binding of estrogens to ERs. However, SERMs may act as partial agonists or exert an estrogenic action in other tissues, leading to an increased risk of endometrial cancer or stroke. An alternative strategy in breast cancer treatment employs aromatase inhibitors (AIs), which lack estrogenic effects and cause fewer side effects.[1] The third-generation AIs, which are now used as first-line therapy in the treatment of early- and advanced-stage breast cancer in postmenopausal women,[2] include two categories: the reversible nonsteroidal inhibitors anastrozole and letrozole (Chart 1) and the steroidal inhibitor exemestane (Chart 1). Nonsteroidal AIs are imidazoles or triazoles that bind to the active site of CYP19 by coordinating the heme iron atom of the enzyme through a heterocyclic nitrogen lone pair. Steroidal inhibitors may exhibit either competitive inhibition, irreversible inhibition, or mechanism-based

inhibition of aromatase. Among them, exemestane is a mechanism-based inhibitor, which is transformed by aromatase into a reactive species that irreversibly binds to the active site of the enzyme. Although AIs are currently popular and effective in the treatment of postmenopausal ER+ breast cancer, the search for novel drugs still remains necessary to avoid the risk of possible emerging resistances to available drugs[3] as well as to reduce toxicity and undesirable side effects associated with a prolonged use.

The publication of a high resolution X-ray structure of human aromatase (PDB code 3EQM, resolution 2.90 Å)[4] has opened the way to a greater understanding of the structural basis for estrogen synthesis and substrate/inhibitor recognition and may encourage efforts to discover novel AIs through structure-based molecular design. So far, new AIs have been mainly designed through ligand-based methods,[5−7] even though docking studies have been performed with homology models of the enzyme.[8,9]

Among structure-based design methods, virtual ligand screening based on flexible docking, i.e., high-throughput docking (HTD), has become a powerful tool for lead discovery. In the past decade, very large databases of commercially available compounds, corporate collections, or virtual libraries have been screened through flexible docking. HTD has been encouraged by an increased availability of structural information on pharmacological targets, advances in computational power, improvements in the efficiency of docking algorithms, as well as in the accuracy of scoring functions and consensus scoring methods.[10]

Here we report the development of an HTD protocol and its application as a virtual screening tool for the identification of

Chart 1. The Third-Generation AIs and the Aromatase Substrate Androstenedione

Anastrozole

Letrozole

Exemestane

Androstenedione
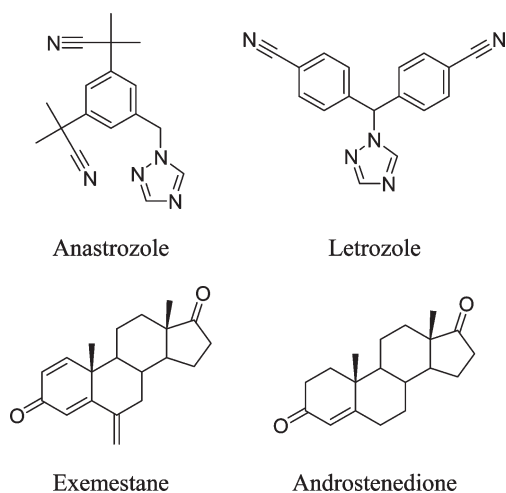
novel nonsteroidal AIs with an imidazole or triazole functional group to coordinate the heme iron. The X-ray structure of human aromatase[4] was used together with a collection of commercially available compounds.

A stepwise filtering protocol based on Lipinski's rule-of-five[11] and additional filters to discard highly flexible compounds and chiral compounds with more than two stereocenters was used to funnel down the number of compounds to be docked. Finally, the compounds selected through the HTD protocol developed in this work were tested for in vitro aromatase inhibition, and highly active AIs with new core structures were identified.

■ RESULTS AND DISCUSSION

So far, structure-based design of new AIs has been hindered by the absence of a crystal structure of this enzyme. However, homology models[12,13] were published and used to perform docking and molecular dynamics simulations on known AIs in order to rationalize mutagenesis data and structure–activity relationships (SAR).[8,9] Ligand-based approaches have therefore been the main strategies employed to identify new AIs.[5−7] However, ligand-based methods are always dependent on the chemical properties of already known inhibitors, thus neglecting to explore new potentially favorable interactions unsatisfied by existing ligands. On the contrary, docking prioritizes ligands with a good functional and steric complementarity with the protein binding site and is not influenced by known ligands.[14] On the other hand, docking protocols are still far from ideal in terms of both managing protein flexibility and the accuracy of the scoring function used to rank ligands. Moreover, in the case of heme proteins, standard docking protocols usually underestimate iron–ligand interactions, even if Morse-like metal binding potentials for docking applications were reported in the literature.[15]

The recent availability of an X-ray structure of human aromatase led us to set up an HTD protocol to identify new chemical scaffolds able to inhibit aromatase, thus testing the possibility of previously unexplored interactions within the aromatase binding site. The Glide software[16,17] was used for docking a collection of commercially available compounds to aromatase. A modified version of ChemScore,[18] GlideScore implemented in Glide, was used to estimate binding affinity and rank ligands.

Before docking libraries of commercially available compounds, the reliability of the chosen docking protocol was tested on a set of known imidazole and triazole AIs from the Binding Database (Binding DB).[19] For some azole inhibitors, including, e.g., anastrozole, both the Glide Standard and Extra Precision[20] docking protocols failed to predict a binding mode where the azole nitrogen coordinates the heme iron. This failure of the docking algorithm in docking azole compounds to heme proteins was also reported by Verras et al.[21] and Potter et al.,[9,22] who used DOCK[23] and GOLD,[24] respectively. Therefore, a docking protocol that included the use of Glide metal constraints was set up. Glide constraints require that a ligand atom lies within a certain region of the binding site in order to interact with specific receptor functionalities. A customized metal constraint was used in order to retrieve ligand poses where an aromatic nitrogen interacts with the heme iron. The use of a distance constraint between the coordinating nitrogen of the azole ring and the iron atom was applied before by Potter et al.[9,22] in their docking studies on AIs. The less CPU-expensive Standard Precision (SP) docking protocol was used instead of the Extra Precision (XP) docking protocol, which failed to generate a pose for some of the known inhibitors from the Binding DB. In fact, the more sophisticated XP scoring function requires a greater protein–ligand shape complementarity and may penalize too much ligands that do not fit well the protein conformation used for docking. A van der Waals radius scaling factor of 0.5 was applied to receptor and ligand radii of atoms with a partial atomic charge (absolute value) less than 0.15. The use of a van der Waals radius scaling factor may partially model protein flexibility, otherwise neglected by rigid protein docking. Including protein flexibility may be particularly important in docking to P450 enzymes. In fact, Verras et al.[21] reported that ketoconazole inhibited both wild-type and L244A P450cam, and that none of the available P450cam crystal structures showed a large enough active site to accommodate such a bulky ligand. Therefore, the authors hypothesized conformational changes in the active site.

The resulting SP docking protocol, which included the metal constraint, was able to generate a pose for each of the azole inhibitors from the Binding DB where the azole ring coordinates the heme iron. Moreover, by using this protocol, the experimentally observed binding mode of bifonazole to cytochrome P450 2B4 (PDB code 2BDM, resolution 2.30 Å) was predicted (rmsd on heavy atoms 1.02 Å) (see Supporting Information).

Asinex Gold and Synergy collections[25] (about 262000 compounds) were searched for imidazole and triazole scaffolds. This choice was based on the knowledge that aromatic nitrogen heterocycles are able to inhibit P450 enzymes by coordinating the heme iron atom, thus preventing oxygen binding and the subsequent oxidation reaction of the substrate.[26] Because the replacement of the imidazole or triazole moiety with a pyridine may result in weaker P450 inhibitors,[27] pyridines were excluded as possible templates, even if pyridyl-substituted AIs are known.[28] Moreover, it was shown that substituents in the α positions with respect to the coordinating nitrogen introduce steric clashes with the heme moiety.[29] Therefore, azoles with a substituent different from a hydrogen in the α positions were excluded. Unhindered imidazoles, 1,2,3 and 1,2,4 triazoles (about 3200 compounds), were extracted from the Asinex collections. Compounds with more than 10 rotatable bonds were filtered out because a high degree of ligand flexibility causes higher entropic penalties upon inhibitor binding and reduces oral bioavailability.[30] Compounds with more than two chiral centers

were excluded as well to avoid synthetic and purification issues. Lipinski's rule-of-five[11] was used to discard compounds with poor absorption and permeation. Finally, compounds were further processed to generate all possible stereoisomers, tautomers, and ionization states at a pH range of 6—8 in order to account for significantly populated species under physiological conditions, leading to about 7000 structures.

The selected azoles were docked into a refined X-ray structure of human aromatase by focusing on the androstenedione binding site and by requiring the satisfaction of the metal constraint. Therefore docked poses that failed to meet the metal binding constraint were rejected. About 2000 structures were filtered out by the docking algorithm, which failed to identify a valid pose after the Glide minimization step or a pose able to satisfy the specified constraint, whereas for the remainder, Glide returned a docking pose and an associated docking score. The selection of compounds for biological evaluation was made by visual inspection of the binding modes because scoring functions are often more successful at predicting a pose than an estimate of the protein—ligand binding energy.[31] Therefore, compounds were prioritized by taking into account their binding mode as well as the overall match among binding modes of all the stereoisomers, tautomers, and ionization states of each compound and, second, their docking score. As for the visual inspection, compounds were checked for a good protein—ligand complementarity. Moreover, ligands able to make interactions with residues known to be important (i) by mutagenesis studies or (ii) because they interact with known substrates/inhibitors were prioritized. Neutral compounds at physiological pH were preferred over charged ones. To promote the selection of structurally diverse compounds, potential hits were grouped into chemical classes by visual inspection, and one molecule was selected for each class. Finally, compounds were checked for readily sample availability from the compound provider, and 17 structurally diverse compounds were purchased and submitted to biological evaluation. All the selected small molecules represent new structural motifs with respect to known AIs.

In vitro aromatase inhibition assays were performed with a semiautomated high-throughput screening method, which employs recombinant human aromatase and a fluorometric substrate, 7-methoxy-4-trifluoromethyl coumarin (MFC), by measuring the reduction in fluorescence associated with the reaction of the MFC substrate.[32] Compounds were assayed as DMSO solutions by maintaining the percentage of DMSO in each well as 0.1%, according to the manufacturer protocol. Letrozole was tested as reference compound and was shown to have an activity comparable to that reported in the literature.[5] Almost all the tested compounds were shown to inhibit aromatase activity at least in the micromolar range, and seven inhibitors were submicromolar hits (Table 1). Compounds 2 (IC_{50} 16.5 nM) and 15 (IC_{50} 9.4 nM) were the most potent compounds with an activity comparable to letrozole (IC_{50} 4.2 nM). Compounds 3 (IC_{50} 119 nM), 5 (IC_{50} 59.2 nM), and 12 (IC_{50} 248 nM) also showed interesting activities. All chiral compounds were purchased and tested as racemic mixtures. In particular, compounds 2, 5, and 15 can exist as couples of enantiomers.

As reported above, cytochromes P450 are characterized by a significant plasticity to accommodate ligands of different sizes. In fact, P450s can adopt multiple conformations depending on the bound ligand. As a consequence, failures in predicting protein—ligand interactions in P450s may be attributed to the use of a single crystal structure of these enzymes.[33] Moreover, the

analysis of the docking poses showed that in some cases polar groups were within hydrogen bond distances but not properly oriented to interact favorably. Therefore, to further account for the binding site flexibility, binding modes of active compounds were regenerated through Glide/Induced Fit Docking (IFD)[34] runs. IFD poses are shown in Figure 1 and discussed hereafter. In general, IFD binding modes were found to show an optimized network of protein—ligand interactions as compared to previous rigid docking results.

Docking results strongly suggested that both the enantiomers of 2, 5, and 15 share a common binding mode to aromatase. All the most active compounds showed a good steric and electronic complementarity with the aromatase active site. In all of them, N3 of an imidazole ring coordinates the heme iron atom, whereas both letrozole and anastrozole, the nonsteroidal AIs in clinical use, interact with the enzyme through a triazole moiety. Interestingly, compounds 3 and 15 are both characterized by the presence of an imidazole group, a sulfonamide group, and three carbon atoms that connect the sulfonamide nitrogen to the imidazole nucleus. In the same way, 5 and 15 share an imidazole ring connected via a methylene to a six-membered ring, a morpholine in 5, whose nitrogen is part of an amide group, and a piperidine in 15, whose nitrogen is part of a sulfonamide. According to the predicted binding modes, each of the most active compounds showed peculiar interactions with the enzyme binding pocket, being the interaction between the azole ring and the heme iron, the hydrogen bond with Met374 NH, and van der Waals interactions with the hydrophobic pocket lined by Ile133, Phe134, Trp224, Val370, Leu372, Val373, Met374, and Leu477 the only interactions conserved among all compounds. Met374 makes a hydrogen bond with the natural substrate androstenedione.[4] In the predicted pose of 15 (Figure 1a), the methoxy oxygen is 3.5 Å from Met374 NH and could make a weak hydrogen bond interaction, while the tert-butyl-methoxy-phenyl moiety interacts with Phe134, Val370, Leu372, Val373, Met374, and Leu477. As shown in Figure 1b, compound 2 p-methoxy substituent forms a hydrogen bond with the backbone NH of Met374, and the p-methoxy phenyl moiety contacts with hydrophobic residues Ile133, Phe134, Val370, Val373, Met374, and Leu477. Compound 5 (Figure 1c) has a trimethoxyphenyl moiety that makes good van der Waals contacts with Ile133, Val370, Leu372, Val373, Met374, and Leu477, while two methoxy oxygens are involved in hydrogen bonds with Met374 NH. The dihydrobenzodioxine moiety of 3 (Figure 1d) makes contact with Phe134, Val370, Leu372, Val373, Met374, and Leu477 and mimics androstenedione D ring, while one of the oxygens of the dihydrobenzodioxine moiety makes a hydrogen bond with Met374 NH. Finally, the fluorophenoxy ring of 12 (Figure 1d) interacts with Phe134, Val370, Val373, Met374, and Leu477, and the fluorine atom is involved in a weak hydrogen bond interaction with Met374 NH.

Hydrogen bonds may also involve Thr310 (2, 5, and 12), Ser478 (3, 15), and to a lesser extent Asp309 (12), while van der Waals contacts are possible with Phe221, Ile305, Ala306, Val313, and Val369. Thr310 represents a highly conserved residue in P450s and is involved together with Ala306 and catalytic water molecules in the aromatase hydroxylation steps.[4] Mutations of Ser478 to alanine or threonine affect letrozole and anastrozole binding.[35] Finally, Asp309 is involved in a hydrogen bond interaction with the natural substrate androstenedione.[4] Moreover, the carboxylate of Asp309 was proposed to participate in the enolization reaction[4] and on the D309A mutant anastrozole

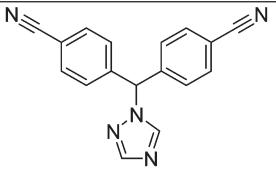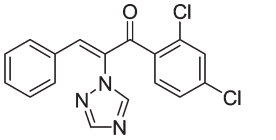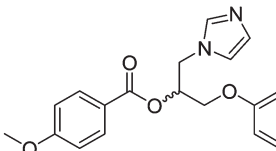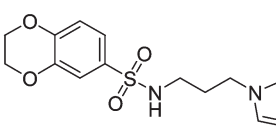## Table 1. Compounds Selected by the High-Throughput Docking Protocol
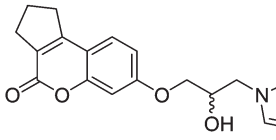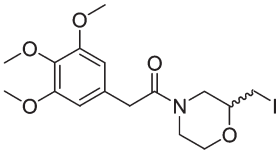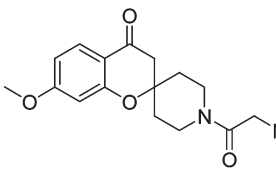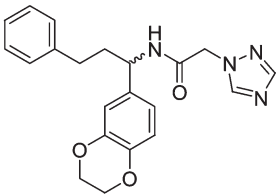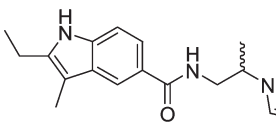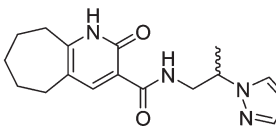
Compound name	Asinex code	Compound structure	IC$_{50}$ (nM)^a
Letrozole^b	/		4.2
1	BAS 00665638		441
2	BAS 02077837		16.5
3	BAS 12756136		119
4	BAS 12914183		21700
5	LEG 13848093		59.2
6	LEG 21508414		5790
7	LEG 22473243		991
8	SYN 15645644		10600
9	SYN 15645717		>25000

Table 1. Continued

Compound name	Asinex code	Compound structure	IC$_{50}$ (nM)^a
10	SYN 17475691		3500
11	SYN 19577078		3100
12	SYN 19990642		248
13	SYN 19994888		non soluble
14	SYN 19999063		3100
15	SYN 20028567		9.4
16	SYN 22987768		non active
17	SYN 23725844		498

^{a} Compounds were tested at a maximum concentration of 25 μM. ^{b} Reference compound.

showed a 7-fold decrease in activity compared to the wild type enzyme.[36] One of the oxygens of the sulphonamide moiety of both **15** and **3** makes a hydrogen bond with Ser478 OH. Moreover, the piperidyl moiety of **15** makes contacts with Ile133, Phe134,
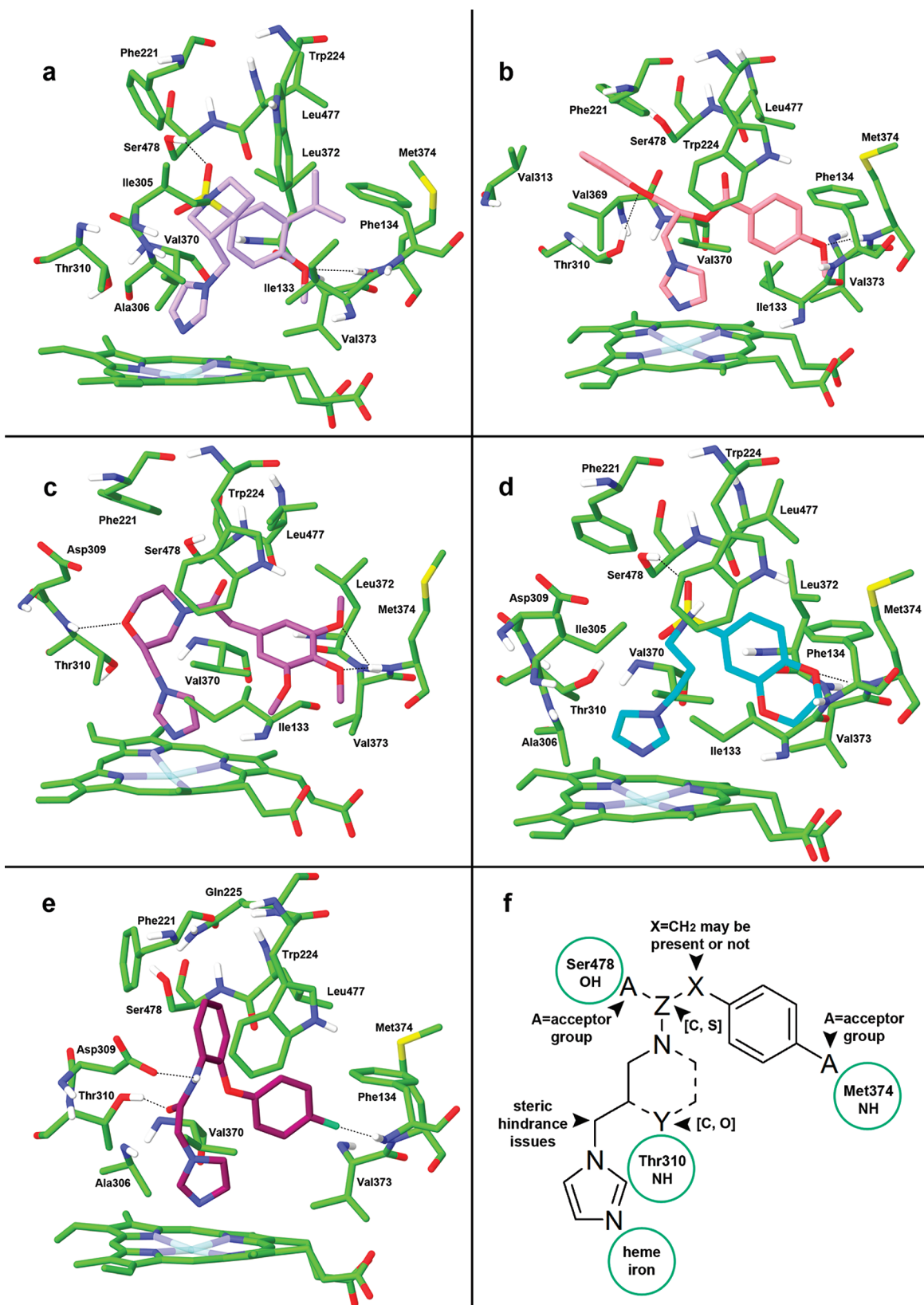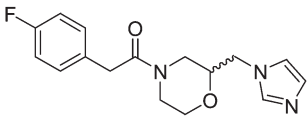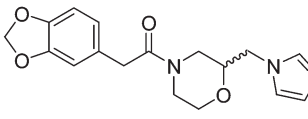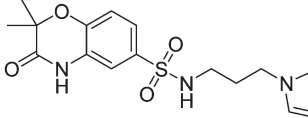
Figure 1. (a) Predicted binding mode of compound **15** (distance Fe−N 2.19 Å). (b) Predicted binding mode of compound **2** (distance Fe−N 2.17 Å). (c) Predicted binding mode of compound **5** (distance Fe−N 2.07 Å). (d) Predicted binding mode of compound **3** (distance Fe−N 2.13 Å). (e) Predicted binding mode of compound **12** (distance Fe−N 2.15 Å). Hydrogen bonds are represented as black dotted lines. (f) SAR of some of the tested compounds.

Table 2. Analogue Compounds

Compound name	Asinex code	Compound structure	IC$_{50}$ (nM)^a
18	AOP 13801200		78.8
19	AOP 13848083		66.5
20	BAS 00782664		1000
21	BAS 05399144		10600
22	BAS 11404029		761
23	BAS 11404034		172
24	BAS 12378719		61.6
25	BAS 12914671		63.7
26	BAS 12914683		440
27	BAS 12927218		2500
28	BAS 15369430		100
29	LEG 20062047		13200

Table 2. Continued

Compound name	Asinex code	Compound structure	IC$_{50}$ (nM)^a
30	SYN 13801197		34.5
31	SYN 13801198		46.7
32	SYN 15516633		499

^{a} Compounds were tested at a maximum concentration of 25 μM.

Phe221, Trp224, Ile305, and Ala306, whereas the alkyl chain of **3**, which connects the imidazole ring to the sulphonamide, contacts with Ile133, Phe221, and Trp224. Both the phenoxy oxygen of **2** and the amide carbonyl of **12** make a hydrogen bond with Thr310 OH, whereas the morpholine oxygen of **5** makes a hydrogen bond with Thr310 NH. Moreover, the phenoxy ring of **2** makes hydrophobic contacts with Phe221, Val313, Val369, and Val370. The morpholine ring of **5** contacts with Phe221, Trp224, and Val370, and the 2-(4-fluorophenoxy) phenyl ring of **12** makes contacts with Phe221, Trp224, the alkyl chain of Gln225, and Leu477. Finally, compound **12** amide NH interacts with the carboxylate oxygen of Asp309 through a hydrogen bond.

The presence of hydrophobic contacts with a considerable number of residues of the highly hydrophobic active site seems to play a pivotal role in compound binding.

Notably, **2** was previously reported as a potential inhibitor of Erg11, which encodes for lanosterol 14α-demethylase, by a yeast-based integrated platform of genomic assays for small-molecule target identification.[37]

■ HIT EXPANSION THROUGH ANALOGUE SEARCH

Encouraged by these initial results, and with the aim of exploring the SAR of the identified hits, commercially available analogue compounds of the most actives were searched among Asinex collections (Elite, Gold, Platinum, and Synergy) and docked to aromatase with the SP docking protocol, as described above. After the visual inspection of the SP docking binding mode for each analogue, a subset of analogues was selected and submitted to IFD. Fifteen compounds were purchased and tested (Table 2). Unfortunately, analogues of compound **2** were not available.

Two analogues of **15** were purchased and tested. Both **18** (IC$_{50}$ 78.8 nM) and **19** (IC$_{50}$ 66.5 nM) were less active than **15** (IC$_{50}$ 9.4 nM). Both compounds differ from the parent compound for the replacement of the piperidine ring with morpholine and for the substituents of the phenyl ring. As a result of the common scaffold, the IFD poses of **18** and **19** within the enzyme binding pocket are similar to that of **15**, even if the absence in **18** and **19** of a lipophilic substituent on the phenyl ring reduces the number of van der Waals contacts with the

hydrophobic pocket lined by Ile133, Phe134, Trp224, Val370, Leu372, Val373, Met374, and Leu477. The loss of these interactions is apparently not counterbalanced by the presence of a stronger hydrogen bond with Met374 NH, involving the methoxy oxygen of **18** (2.8 Å) and the carbonyl oxygen of the acetophenone moiety of **19** (3.1 Å), respectively.

Seven analogues of **3** (IC$_{50}$ 119 nM) were purchased and tested (**22**, **23**, **24**, **25**, **26**, **28**, **32**). Four compounds, namely **23** (IC$_{50}$ 172 nM), **24** (IC$_{50}$ 61.6 nM), **25** (IC$_{50}$ 63.7 nM), and **28** (IC$_{50}$ 100 nM), showed an activity comparable to that of **3**, being **24** and **25** the most active compounds of the series, whereas **23** was less active than **3**. According to the IFD results, all these compounds bind to aromatase in a similar way to that of **3**, the hydrogen bond with Ser478 is conserved as well as the good van der Waals contacts with the hydrophobic pocket, while the hydrogen bond with Met374 is lost in **23**, thus accounting for its lower affinity. Compounds **22** (IC$_{50}$ 761 nM), **26** (IC$_{50}$ 440 nM), and **32** (IC$_{50}$ 499 nM) were less active than **3**. Interestingly, **26** (IC$_{50}$ 440 nM) differs from **15** (IC$_{50}$ 9.4 nM) for the replacement of the piperidine ring with the flexible alkylic chain, characteristic of the parent compound **3**. In this case, the greater rigidity of **15** reduces entropic penalties. Moreover, by analyzing the predicted pose of **26**, the decrease in activity observed when the methyl substituent of **24** is replaced by the bulkier *tert*-butyl group of **26** may be ascribed to steric bumps with Val373, Leu477, and the heme moiety. Such bumps are absent in **15** as a result of the partly different scaffold and, consequently, the partly different binding mode. Compound **22** (IC$_{50}$ 761 nM) has a bicyclic system connected to the sulfonamide as in **3**, although there is a shift in the ring substitution pattern (the sulphonamide is shifted from the β to the α position of the bicyclic ring). Moreover, the bicyclic system is a 4-ethoxynaphtalene instead of a dihydrobenzodioxine. The lower affinity of **22** can be explained by steric hindrance caused by the bicyclic system that impedes the formation of the conserved hydrogen bond with Met374 NH. The predicted binding mode of **32** (IC$_{50}$ 499 nM) shows that the compound, although conserving the above-mentioned interactions, points the amide NH as well as the ether oxygen, which are not involved in hydrogen bonds, in a hydrophobic region, thus desolvation penalties may arise.

Table 3. Properties of Tested Compounds Calculated by QikProp

compd	Asinex code	molecular weight[a]	QPlogPo/w[b]	QPlogS[c]	QPPCaco2[d]	no. of primary metabolites[e]
1	BAS 00665638	344.2	3.94	−4.4	1725	0
2	BAS 02077837	352.4	3.73	−3.3	2185	2
3	BAS 12756136	323.4	1.18	−1.4	940	0
4	BAS 12914183	327.3	1.58	−3.3	347	4
5	LEG 13848093	375.4	1.16	−0.4	1169	5
6	LEG 21508414	356.4	0.38	−0.9	287	3
7	LEG 22473243	378.4	2.64	−2.2	1454	3
8	SYN 15645644	311.4	3.14	−4.2	1242	2
9	SYN 15645717	315.4	2.32	−3.9	367	2
10	SYN 17475691	339.4	2.36	−2.3	1145	8
11	SYN 19577078	390.5	2.66	−2.7	1074	5
12	SYN 19990642	311.3	3.22	−3.5	2453	2
13	SYN 19994888	399.9	3.28	−4.8	1195	3
14	SYN 19999063	354.4	3.61	−4.0	3222	3
15	SYN 20028567	391.5	2.94	−2.9	1317	2
16	SYN 22987768	407.5	4.37	−5.0	4043	1
17	SYN 23725844	368.4	3.94	−4.0	3201	2
18	AOP 13801200	337.4	0.68	−0.3	1258	2
19	AOP 13848083	349.4	0.00	−0.1	458	1
20	BAS 00782664	288.3	1.97	−2.5	591	2
21	BAS 05399144	244.3	1.90	−2.3	1464	2
22	BAS 11404029	359.4	2.61	−2.6	1251	1
23	BAS 11404034	307.4	2.07	−2.4	1095	3
24	BAS 12378719	309.4	1.79	−2.1	1305	2
25	BAS 12914671	364.2	2.16	−2.3	1352	1
26	BAS 12914683	351.5	2.47	−2.5	986	2
27	BAS 12927218	362.4	1.94	−2.3	766	1
28	BAS 15369430	313.3	1.48	−1.7	878	1
29	LEG 20062047	340.4	3.39	−3.2	3213	1
30	SYN 13801197	303.3	1.42	−0.8	1625	2
31	SYN 13801198	329.4	1.05	−0.8	1106	2
32	SYN 15516633	364.4	1.12	−2.6	449	1

[a] Range 95% of drugs (130/725). [b] Log of the octanol/water partition coefficient, range 95% of drugs (−2/6.5). [c] Log of aqueous solubility S (mol/L), range 95% of drugs (−6.5/0.5). [d] Caco2 cell permeability in nm/s, range 95% of drugs (<25 poor, >500 great). [e] Range 95% of drugs (1/8).

To examine the role of the sulfonamide group, three compounds, namely **20** (IC_{50} 1000 nM), **21** (IC_{50} 10600 nM), and **27** (IC_{50} 2500 nM), where the sulfonamide was replaced by an amide, were tested. These compounds also differ from **3, 15**, and their analogues for the substituents on the phenyl ring connected to the sulphonamide/amide, nonetheless they present polar moieties capable of hydrogen bonding with Met374 as well as lipophilic groups that make good contacts with the hydrophobic pocket. Direct comparisons between compounds that differ only for the replacement of the sulfonamide with the amide were not possible as a result of the limited chemical space available within the commercial collections. All of them were less active than the sulfonamide derivatives. Compound **20** makes two hydrogen bonds with Ser478 OH and Met374 NH. Compound **21** loses the hydrogen bond with Met374 NH, while **27** makes two hydrogen bonds with Met374 NH and Ser478 OH as well as good van der Waals contacts that involve the allylic chain. Accordingly, it seems that the hydrogen bond between Ser478 and the sulfonamide is stronger and/or geometrically favored with respect to that with the amide, being all other interactions conserved at least in **27**.

Compound **29** (IC_{50} 13200 nM) was the only analogue of **12** (IC_{50} 248 nM) that was purchased and tested. Its binding mode is similar to that of **12**, being the substitution of the imidazole ring with a triazole and the dimethyl substituent on the propanamide chain the only differences between the two. However, the steric hindrance caused by the dimethyl substituent allows for the formation of only a hydrogen bond with Thr310 OH instead of two with Thr310 OH and the carboxylate of Asp309 as in **12**. Moreover, the replacement of the imidazole ring of **12** with the triazole of **29** may be detrimental to activity. Even if third-generation AIs used in therapy are triazole derivatives, the loss of activity caused by the replacement of an imidazole nucleus with a triazole was observed for other P450 inhibitors.[38] In fact, the presence of a free triazole nitrogen atom that does not make hydrogen bonds with a protein residue and remains essentially unsolvated may result in a higher desolvation penalty upon binding.[39]

Both analogues of **5** (IC_{50} 59.2 nM), i.e., **30** (IC_{50} 34.5 nM) and **31** (IC_{50} 46.7 nM), were slightly more potent than the parent compound. According to the IFD results, compounds **30** and **31** form three hydrogen bonds with Thr310 NH, Met374

NH, and Ser478 OH. Therefore, the geometric requirements of the amide group in the six-membered ring of **30** and **31** still allow a strong hydrogen bond interaction with Ser478 OH, as in the case of sulfonamide containing compounds.

In summary, the conclusions that can be drawn by the new identified AIs are that, in addition to the interaction between the azole rings and the heme iron, hydrophobic contacts play a pivotal role in ligand binding, and two or three hydrogen bonds involving Asp309, Thr310, Met374, or Ser478 are essential for ligand recognition. In particular, part of the SAR of the most active compounds is summarized in Figure 1f by using the scaffold of **3**, **5**, **15**, and their analogues. As shown in Figure 1f, the presence in **30** and **31** of a methylene spacer (X) between the acceptor group that interacts with Ser478 and the phenyl ring bearing the acceptor interacting with Met374 shortens the distance between the second acceptor group and Met374 NH and could lead to a stronger hydrogen bond and, consequently, more active derivatives also in the series of **15**. Moreover, it could be hypothesized that the steric hindrance on the carbon connected to the azole nucleus as in **29** could be detrimental to activity also in other classes of compounds, as in the case of **8** (IC_{50} 10600 nM) and **9** (IC_{50} >25000 nM). Finally, the presence of a morpholine instead of a piperidine leads in **5**, **30**, and **31** to an additional hydrogen bond with Thr310 NH, whereas this is not the case in **18** and **19**. In fact, as a result of the absence in **18** and **19** of the methylene linker, the molecule adopts a partly different binding mode in order to interact with Met374 and the morpholine oxygen is far from Thr310.

To assess the novelty of the tested compounds with respect to known AIs, pairwise Tanimoto similarity indices for each of the tested compounds with imidazole and triazole AIs from the Binding DB were calculated through a python script by using the default fingerprint module of the RDKit suite.[40] In addition to Binding DB compounds, two recently identified inhibitors, a bicyclic derivative of the potent dual aromatase-steroid sulfatase inhibitor 2-bromo-4-{[(4-cyanophenyl)(4H-1,2,4-triazol-4-yl)-amino]methyl}phenylsulfamate (compound **39** in the original paper),[41] and a resveratrol analogue (compound **82** in the original paper),[42] were included in the pool of known AIs. All the tested compounds exhibited low Tanimoto similarity indices (ranging from 0.19 to 0.68) to each of the known AIs. The maximum similarity index was observed between **4** and a coumarin derivative. In particular, the ranges for the most active compounds **2** (0.21−0.52), **3** (0.21−0.48), **5** (0.23−0.55), **12** (0.20−0.46), **15** (0.23−0.59), **18** (0.21−0.53), **19** (0.22−0.55), **24** (0.22−0.45), **25** (0.20−0.50), **30** (0.22−0.48), and **31** (0.22−0.55) were even smaller. Accordingly, the newly identified hits can be considered as novel.

Finally, expected ADME properties of the tested compounds were evaluated with QikProp[16] and are reported in Table 3. The selected properties are known to influence metabolism, cell permeation, and bioavailability.[43] Almost all the predicted properties of the tested compounds were in the ranges predicted by QikProp for 95% of known oral drugs. Compound **3** has no predicted primary metabolites, but its analogues, including **24** and **25**, the most active compounds of the series, have a number of primary metabolites in the allowed range (1−8).

■ CONCLUSIONS

A successful HTD screening of a library of commercially available compounds was set up by using the recently published crystallographic structure of aromatase. Highly active inhibitors with new structural motifs, as for example the sulfonamide containing compounds **3**, **15**, **18**, **19**, **24**, and **25**, the morpholino ethanone derivatives **5**, **30**, and **31** and the imidazolyl acetamide compound **12** were identified. Compound **2** as well is different from all known AIs, but it could be a potential inhibitor of other P450s.[37] Subsequent hit expansion through analogue search allowed us to explore the SAR of the identified inhibitors and yielded some compounds with improved activity with respect to the parent compound as in the case of **24**, **25**, **30**, and **31**. Binding modes of actives compounds were further confirmed with IFD, thus accounting for protein flexibility that plays an important role in protein−ligand recognition, particularly in highly flexible active sites such as those of P450s. The properties of these hit compounds warrant further biological characterization as cellular assays to confirm in vivo their interesting in vitro profile. Moreover, synthetic efforts will be pursued to yield small sublibraries of the most active inhibitors, particularly analogues of compound **2** that were not commercially available, to further explore their SAR.

■ EXPERIMENTAL SECTION

Ligand Preparation and Filtering. Three-dimensional structures of Asinex Gold and Synergy compounds[25] were extracted from the CoCoCo database[44] after the first conversion step (i.e., 2D structures were converted into their corresponding 3D structures, hydrogens were added, and all but the largest fragments were removed from multicomponent records by Corina 3.48[45,46]). Compounds were then filtered through the Schrödinger Suite 2008 Ligfilter tool[16] in order to retrieve compounds containing imidazole or 1,2,3 and 1,2,4 triazole rings (with hydrogen atoms bound to the α positions with respect to the nitrogen that has to coordinate the heme iron), thus collecting about 3200 compounds. Compounds with more than 10 rotatable bonds and two chiral centers were removed, as well as compounds that violate Lipinski's rule-of-five.[11] The octanol/water partition coefficient (QPlogPo/w) predicted by Qikprop v31207[16] was considered as the LogP value. Stereoisomers were generated with Corina 3.48 and a maximum number of two stereocenters were processed, leading to a maximum number of four stereoisomeric compounds for each entry.

To set the ionization and tautomerization state of compounds at a pH range of 6−8, Epik v16207[16] was used, with a maximum number of four generated structures per input structure.

Then, compounds were minimized with the Schrödinger Suite 2008 premin tool[16] (MMFF force field). About 7000 structures, including stereoisomers, tautomers, and ionization states, were ready to be submitted to the subsequent docking run.

Protein Preparation. The X-ray coordinates of human aromatase in complex with androstenedione were extracted from the Protein Data Bank (PDB code 3EQM).[4] The structure was then processed with the Schrödinger Suite 2008 Protein Preparation Wizard tool.[16] This tool automatically sets a charge (+3) and a correct atom type to the iron atom, bond orders and formal charges to the heme moiety, and the orientation of any misoriented groups (such as amide groups of Asn and Gln). Cys437 was considered as a negatively charged cysteine thiolate axial ligand of the heme iron. The substrate and water molecules were removed, and an exhaustive sampling of the orientations of groups, whose hydrogen bonding network needs to be optimized, was performed. Finally, the protein structure was refined to relieve steric clashes with a restrained minimization with the OPLS2001 force field until a final rmsd of 0.030 Å with respect to the input protein coordinates.

Docking. Docking studies were performed using Glide v50208.[16,17] The protein structure, prepared as described above, was used to build the

energy grid. A van der Waals radius scaling factor of 0.50 for atoms with a partial atomic charge (absolute value) less than 0.15 was used in order to soften the potential for nonpolar parts of the receptor. The enclosing box was centered on the heme residue, and default sizes were used for both the enclosing and bounding box. The SP docking protocol was used. The satisfaction of a Glide constraint, i.e., a ligand—receptor interaction requirement, was incorporated into Glide hierarchical filters by allowing the rejection of docked poses that failed to meet such a requirement. In particular, a metal constraint was used in order to retrieve ligand poses where an aromatic nitrogen atom interacts with the heme iron. The ligand nitrogen must be within 2.4 Å of the metal in order to satisfy the constraint. Ligands were docked flexibly, the sampling of ring conformations was included, and nonplanar amide conformations were penalized. SP docking was performed selecting 1000 poses per ligand to be energy minimized on the OPLS-AA nonbonded-interaction grid and a van der Waals radius scaling factor of 0.5 for ligand atoms with a partial atomic charge (absolute value) less than 0.15. All other parameters were set to their default value. The docking protocol was validated by using a set of AIs from the Binding DB.[19] Different protocols were tested for their ability to return binding modes where azole inhibitors coordinate the heme iron. Moreover, it was verified that for analogue compounds a similar binding mode was shared among the series and that anastrozole binding mode was consistent with available mutagenesis data.[35,36]

Docking results were sorted by GlideScore and top ranked compounds were visually inspected. Seventeen compounds were selected, purchased, and submitted to biological evaluation.

Induced Fit Docking (v08208)[34]. An initial Glide SP docking of each ligand was performed by using a softened potential, i.e., a van der Waals radius scaling factor of 0.50 for receptor/ligand atoms with a partial atomic charge (absolute value) less than 0.15, the metal constraint, and a number of 1000 poses per ligand to be energy minimized on the OPLS-AA nonbonded-interaction grid, as reported above. One hundred poses were saved for each ligand and submitted to the subsequent Prime[16] side-chain orientation prediction of residues within a shell of 6 Å around each ligand. After the Prime minimization of the selected residues and the ligand for each pose, a Glide redocking of each protein—ligand complex structure within 30 kcal/mol of the lowest energy structure was performed. Finally, binding energy (IFDScore) for each output pose was estimated and the poses for each protein—ligand complex were visually inspected.

ADME Properties Prediction. ADME properties for tested compounds were evaluated by using Qikprop v31207.[16]

In Vitro Aromatase Inhibition Assays. The tested compounds were purchased from Asinex.[25] The vendor had verified compound purity by liquid chromatography—mass spectrometry (LC-MS) or nuclear magnetic resonance (NMR) experiments. All compounds had at least 95% purity except **2** (93%), **24** (91%), and **25** (93%). All chiral compounds were purchased and tested as racemic mixtures. Compound **1** was purchased and tested as a mixture of 67% *Z* isomer and 33% *E* isomer, while compound **11** was a mixture of *trans* isomers. Compounds **10**, **17**, and **18** were purchased as salts of $C(OH)(CH_2CO_2H)_2CO_2H$, HCl, and $4\text{-}CH_3C_6H_4SO_3H$, respectively.

In vitro aromatase inhibition assays were performed by using the CYP19/MFC High Throughput Inhibitor Screening Kit (aromatase activity = 2.8 pmol product/(min × pmol P450); protein content = 6.9 mg/mL; BD Biosciences, Oxford, UK). MFC was used as substrate for the reaction. Enzyme reactions were performed in BD Falcon 96-well black plates (BD Biosciences, Oxford, UK). Compounds were tested in DMSO, taking care that the final percentage of DMSO in each well was 0.1%. A percentage of DMSO higher than 0.2% was found to inhibit aromatase activity and was avoided. Fluorescence measurements were recorded by using a Tecan GENios Pro plate reader, with a number of reads per well of 10, an excitation wavelength of 405 nm, and an emission wavelength of 535 nm. Assays were performed in duplicate. Blank values were subtracted from the sample wells to obtain the net fluorescence signal. The values were normalized to those obtained without inhibitor addition, and results were expressed as percentage of inhibition. Dose—response curves were fitted with Graphpad Prism 4.0c.[47] Letrozole (Altan Corporation, Orange CT, USA) was used as standard compound.

■ ASSOCIATED CONTENT

ⓢ Supporting Information. Predicted binding mode of bifonazole to cytochrome P450 2B4 and of anastrozole to aromatase. Concentration—response plots of virtual screening hits and analogue compounds. This material is available free of charge via the Internet at http://pubs.acs.org.

■ AUTHOR INFORMATION

Corresponding Author

*Phone: +39 051 2094004. Fax: +39 051 2094746. E-mail: alberto.delrio@gmail.com. Current address: Department of Experimental Pathology, Alma Mater Studiorum, University of Bologna, Via S. Giacomo 14, 40126 Bologna, Italy.

■ ACKNOWLEDGMENT

■ ABBREVIATIONS

AIs, aromatase inhibitors; CYP19, cytochrome P450 aromatase; ER, estrogen receptor; SERMs, selective estrogen receptor modulators; HTD, high-throughput docking; SAR, structure—activity relationships; Binding DB, Binding Database; SP, Standard Precision; XP, Extra Precision; MFC, 7-methoxy-4-trifluoromethyl coumarin; IFD, Induced Fit Docking

■ REFERENCES

(1) Macedo, L. F.; Sabnis, G.; Brodie, A. Aromatase inhibitors and breast cancer. *Ann. N. Y. Acad. Sci.* **2009**, *1155*, 162–173.

(2) Hong, Y.; Chen, S. Aromatase inhibitors: structural features and biochemical characterization. *Ann. N.Y. Acad. Sci.* **2006**, *1089*, 237–251.

(3) Dutta, U.; Pant, K. Aromatase inhibitors: past, present and future in breast cancer therapy. *Med. Oncol.* **2008**, *25*, 113–124.

(4) Ghosh, D.; Griswold, J.; Erman, M.; Pangborn, W. Structural basis for androgen specificity and oestrogen synthesis in human aromatase. *Nature* **2009**, *457*, 219–223.

(5) Schuster, D.; Laggner, C.; Steindl, T. M.; Palusczak, A.; Hartmann, R. W.; Langer, T. Pharmacophore modeling and in silico screening for new P450 19 (aromatase) inhibitors. *J. Chem. Inf. Model.* **2006**, *46*, 1301–1311.

(6) Neves, M. A.; Dinis, T. C.; Colombo, G.; Sá e Melo, M. L. Fast three dimensional pharmacophore virtual screening of new potent non-steroid aromatase inhibitors. *J. Med. Chem.* **2009**, *52*, 143–150.

(7) Neves, M. A.; Dinis, T. C.; Colombo, G.; Sá e Melo, M. L. An efficient steroid pharmacophore-based strategy to identify new aromatase inhibitors. *Eur. J. Med. Chem.* **2009**, *44*, 4121–4127.

(8) Gobbi, S.; Cavalli, A.; Negri, M.; Schewe, K. E.; Belluti, F.; Piazzi, L.; Hartmann, R. W.; Recanatini, M.; Bisi, A. Imidazolylmethylbenzophenones as highly potent aromatase inhibitors. *J. Med. Chem.* **2007**, *50*, 3420–3422.

(9) Jackson, T.; Woo, L. W.; Trusselle, M. N.; Purohit, A.; Reed, M. J.; Potter, B. V. L. Non-steroidal aromatase inhibitors based on a

biphenyl scaffold: synthesis, in vitro SAR, and molecular modelling. *ChemMedChem* **2008**, No. 3, 603–618.

(10) Alvarez, J. C. High-throughput docking as a source of novel drug leads. *Curr. Opin. Chem. Biol.* **2004**, *8*, 365–370.

(11) Lipinski, C. A.; Lombardo, F.; Dominy, B. W.; Feeney, P. J. Experimental and computational approaches to estimate solubility and permeability in drug discovery and development settings. *Adv. Drug. Delivery Rev.* **1997**, *23*, 3–25.

(12) Favia, A. D.; Cavalli, A.; Masetti, M.; Carotti, A.; Recanatini, M. Three-dimensional model of the human aromatase enzyme and density functional parameterization of the iron-containing protoporphyrin IX for a molecular dynamics study of heme-cysteinato cytochromes. *Proteins* **2006**, *62*, 1074–1087.

(13) Karkola, S.; Höltje, H. D.; Wähälä, K. J. A three-dimensional model of CYP19 aromatase for structure-based drug design. *Steroid Biochem. Mol. Biol.* **2007**, *105*, 63–70.

(14) Steindl, T.; Langer, T. Docking versus pharmacophore model generation: a comparison of high-throughput virtual screening strategies for the search of human rhinovirus coat protein inhibitors. *QSAR Comb. Sci.* **2005**, *24*, 470–479.

(15) Röhrig, U. F.; Grosdidier, A.; Zoete, V.; Michielin, O. Docking to heme proteins. *J. Comput. Chem.* **2009**, *3*, 2305–2315.

(16) *Schrödinger*; Schrödinger LLC: New York, 2005; http://www.schrodinger.com.

(17) Friesner, R. A.; Banks, J. L.; Murphy, R. B.; Halgren, T. A.; Klicic, J. J.; Mainz, D. T.; Repasky, M. P.; Knoll, E. H.; Shelley, M.; Perry, J. K.; Shaw, D. E.; Francis, P.; Shenkin, P. S. Glide: A new approach for rapid, accurate docking and scoring. 1. Method and assessment of docking accuracy. *J. Med. Chem.* **2004**, *47*, 1739–1749.

(18) Eldridge, M. D.; Murray, C. W.; Auton, T. R.; Paolini, G. V.; Mee, R. P. Empirical scoring functions: I. The development of a fast empirical scoring function to estimate the binding affinity of ligands in receptor complexes. *J. Comput.-Aided Mol. Des.* **1997**, *11*, 425–445.

(19) Chen, X.; Liu, M.; Gilson, M. K. Binding DB: a web-accessible molecular recognition database. *Comb. Chem. High Throughput Screening* **2001**, *4*, 719–725; http://www.bindingdb.org (accessed May 5, 2009).

(20) Friesner, R. A.; Murphy, R. B.; Repasky, M. P.; Frye, L. L.; Greenwood, J. R.; Halgren, T. A.; Sanschagrin, P. C.; Mainz, D. T. Extra precision glide: docking and scoring incorporating a model of hydrophobic enclosure for protein–ligand complexes. *J. Med. Chem.* **2006**, *49*, 6177–6196.

(21) Verras, A.; Kuntz, I. D.; Ortiz de Montellano, P. R. Computer-assisted design of selective imidazole inhibitors for cytochrome p450 enzymes. *J. Med. Chem.* **2004**, *47*, 3572–3579.

(22) Woo, L. W. L.; Bubert, C.; Sutcliffe, O. B.; Smith, A.; Chander, S. K.; Mahon, M. F.; Purohit, A.; Reed, M. J.; Potter, B. V. L. Dual aromatase–steroid sulfatase inhibitors. *J. Med. Chem.* **2007**, *50*, 3540–3560.

(23) Ewing, T. J.; Makino, S.; Skillman, A. G.; Kuntz, I. D. DOCK 4.0: search strategies for automated molecular docking of flexible molecule databases. *J. Comput.-Aided Mol. Des.* **2001**, *15*, 411–428.

(24) Jones, G.; Willett, P.; Glen, R. C.; Leach, A. R.; Taylor, R. Development and validation of a genetic algorithm for flexible docking. *J. Mol. Biol.* **1997**, *267*, 727–748.

(25) *Asinex*; Asinex Ltd: Moscow; http://www.asinex.com.

(26) Testa, B.; Jenner, P. Inhibitors of cytochrome P-450s and their mechanism of action. *Drug Metab. Rev.* **1981**, *12*, 1–117.

(27) Balding, P. R.; Porro, C. S.; McLean, K. J.; Sutcliffe, M. J.; Maréchal, J. D.; Munro, A. W.; de Visser, S. P. How do azoles inhibit cytochrome P450 enzymes? A density functional study. *J. Phys. Chem. A* **2008**, *112*, 12911–12918.

(28) Hartmann, R. W.; Bayer, H.; Grün, G.; Sergejew, T.; Bartz, U.; Mitrenga, M. Pyridyl-substituted tetrahydrocyclopropa[a]naphthalenes: highly active and selective inhibitors of P450 arom. *J. Med. Chem.* **1995**, *38*, 2103–2111.

(29) Rogerson, T. D.; Wilkinson, C. F.; Hetarski, K. Steric factors in the inhibitory interaction of imidazoles with microsomal enzymes. *Biochem. Pharmacol.* **1977**, *26*, 1039–1042.

(30) Veber, D. F.; Johnson, S. R.; Cheng, H. Y.; Smith, B. R.; Ward, K. W.; Kopple, K. D. Molecular properties that influence the oral bioavailability of drug candidates. *J. Med. Chem.* **2002**, *45*, 2615–2623.

(31) Jacobsson, M.; Gäredal, M.; Schultz, J.; Karlén, A. Identification of *Plasmodium falciparum* spermidine synthase active site binders through structure-based virtual screening. *J. Med. Chem.* **2008**, *51*, 2777–2786.

(32) Stresser, D. M.; Turner, S. D.; McNamara, J.; Stocker, P.; Miller, V. P.; Crespi, C. L.; Patten, C. J. A high-throughput screen to identify inhibitors of aromatase (CYP19). *Anal. Biochem.* **2000**, *284*, 427–430.

(33) Zhao, Y.; White, M. A.; Muralidhara, B. K.; Sun, L.; Halpert, J. R.; Stout, C. D. Structure of microsomal cytochrome P450 2B4 complexed with the antifungal drug bifonazole: insight into P450 conformational plasticity and membrane interaction. *J. Biol. Chem.* **2006**, *281*, 5973–5981.

(34) Sherman, W.; Day, T.; Jacobson, M. P.; Friesner, R. A.; Farid, R. Novel procedure for modeling ligand/receptor induced fit effects. *J. Med. Chem.* **2006**, *49*, 534–553.

(35) Kao, Y. C.; Korzekwa, K. R.; Laughton, C. A.; Chen, S. Evaluation of the mechanism of aromatase cytochrome P450. A site-directed mutagenesis study. *Eur. J. Biochem.* **2001**, *268*, 243–251.

(36) Kao, Y. C.; Cam, L. L.; Laughton, C. A.; Zhou, D.; Chen, S. Binding characteristics of seven inhibitors of human aromatase: a site-directed mutagenesis study. *Cancer Res.* **1996**, *56*, 3451–3460.

(37) Hoon, S.; Smith, A. M.; Wallace, I. M.; Suresh, S.; Miranda, M.; Fung, E.; Proctor, M.; Shokat, K. M.; Zhang, C.; Davis, R. W.; Giaever, G.; St Onge, R. P.; Nislow, C. An integrated platform of genomic assays reveals small-molecule bioactivities. *Nature Chem. Biol.* **2008**, *4*, 498–506.

(38) La Regina, G.; D'Auria, F. D.; Tafi, A.; Piscitelli, F.; Olla, S.; Caporuscio, F.; Nencioni, L.; Cirilli, R.; La Torre, F.; De Melo, N. R.; Kelly, S. L.; Lamb, D. C.; Artico, M.; Botta, M.; Palamara, A. T.; Silvestri, R. 1-[(3-Aryloxy-3-aryl)propyl]-1*H*-imidazoles, new imidazoles with potent activity against *Candida albicans* and dermatophytes. Synthesis, structure–activity relationship, and molecular modeling studies. *J. Med. Chem.* **2008**, *51*, 3841–3855.

(39) Poulos, T. L.; Howard, A. J. Crystal structures of metyrapone-and phenylimidazole-inhibited complexes of cytochrome P-450cam. *Biochemistry* **1987**, *26*, 8165–8174.

(40) *RDKit: Cheminformatics and Machine Learning Software*; Sourceforge; http://www.rdkit.org.

(41) Wood, P. M.; Woo, L. W.; Labrosse, J. R.; Thomas, M. P.; Mahon, M. F.; Chander, S. K.; Purohit, A.; Reed, M. J.; Potter, B. V. L. Bicyclic derivatives of the potent dual aromatase-steroid sulfatase inhibitor 2-bromo-4-{[(4-cyanophenyl)(4*H*-1,2,4-triazol-4-yl)amino]-methyl}phenylsulfamate: synthesis, SAR, crystal structure, and in vitro and in vivo activities. *ChemMedChem* **2010**, No. 5, 1577–1593.

(42) Sun, B.; Hoshino, J.; Jermihov, K.; Marler, L.; Pezzuto, J. M.; Mesecar, A. D.; Cushman, M. Design, synthesis, and biological evaluation of resveratrol analogues as aromatase and quinone reductase 2 inhibitors for chemoprevention of cancer. *Bioorg. Med. Chem.* **2010**, *18*, 5352–5366.

(43) Ravindranathan, K. P.; Mandiyan, V.; Ekkati, A. R.; Bae, J. H.; Schlessinger, J.; Jorgensen, W. L. Discovery of novel fibroblast growth factor receptor 1 kinase inhibitors by structure-based virtual screening. *J. Med. Chem.* **2010**, *53*, 1662–1672.

(44) Del Rio, A.; Barbosa, A. J.; Caporuscio, F.; Mangiatordi, G. F. CoCoCo: a free suite of multiconformational chemical databases for high-throughput virtual screening purposes. *Mol. Biosyst.* **2010**, *6*, 2122–2128; http://www.cococo-database.it (release 2010).

(45) *Molecular Networks: Inspiring Chemical Discovery*; Molecular Networks GmbH—Computerchemie, Erlangen, Germany; http://www.molecular-networks.com.

(46) Gasteiger, J.; Rudolph, C.; Sadowski, J. Automatic generation of 3D-atomic coordinates for organic molecules. *Tetrahedron Comput. Methods* **1990**, *3*, 537–547.

(47) *GraphPad Software*; GraphPad Software: San Diego, CA; www.graphpad.com.